JOURNAL OF GEOPHYSICAL RESEARCH, VOL. 114, D02103, doi:10.1029/2008JD010045, 2009

Boreal spring Southern Hemisphere Annular Mode, Indian Ocean sea surface temperature, and East Asian summer monsoon

Sulan Nan,[1,2] Jianping Li,[3] Xiaojun Yuan,[4] and Ping Zhao[1,2]

Received 29 February 2008; revised 23 October 2008; accepted 3 November 2008; published 22 January 2009.

[1] The relationships among the boreal spring Southern Hemisphere Annular Mode (SAM), the Indian Ocean (IO) sea surface temperature (SST), and East Asian summer monsoon (EASM) are examined statistically in this paper. The variability of boreal spring SAM is closely related to the IO SST. When the SAM is in its strong positive phase in boreal spring, with low-pressure anomalies over the south pole and high-pressure anomalies over middle latitudes, SST over the subtropics and middle latitudes of the South Indian Ocean (SIO) increases, which persists into the summer. Following the positive SST anomalies over the subtropics and midlatitudes of the SIO, SST in the equatorial Indian Ocean and Bay of Bengal increases in summer. Moreover, the variability of SST in the equatorial Indian Ocean and Bay of Bengal is closely related to EASM. When SST in the equatorial Indian Ocean and Bay of Bengal increases, EASM tends to be weak. Therefore the IO SST may play an important role bridging boreal spring SAM and EASM. The atmospheric circulations and surface heat exchanges contribute to the SST anomalies in the SIO. When the spring SAM is in its strong positive phases, the regional Ferrel Cell weakens, and the anomalous upward motions at 20°S–30°S cause an increase of low cloud cover and downward longwave radiation flux. The surface atmospheric circulations also transport more (less) warmer (cooler) air from middle latitudes north of 50°S (high latitudes south of 60°S) into 50°S–60°S and warm the air, which reduces the temperature difference between the ocean and atmosphere and consequently reduces sensible heat flux from the ocean to atmosphere. The increased downward longwave radiation and decreased sensible heat are responsible for the SST increase in the SIO. The atmospheric circulation and surface heat flux anomalies are of opposite signs following the strong negative phases of SAM.

Citation: Nan, S., J. Li, X. Yuan, and P. Zhao (2009), Boreal spring Southern Hemisphere Annular Mode, Indian Ocean sea surface temperature, and East Asian summer monsoon, *J. Geophys. Res.*, *114*, D02103, doi:10.1029/2008JD010045.

1. Introduction

[2] The Southern Hemisphere Annular Mode (SAM), referred to as Antarctic oscillation (AAO), is a pattern which involves a zonally symmetric seesaw in sea level pressure (SLP) and geopotential height between the southern polar region and middle latitudes. It explains the greatest proportion of the total variance of the Southern Hemisphere (SH) monthly SLP, zonal wind and geopotential height [*Kidson*, 1975; *Rogers and van Loon*, 1982; *Gong and Wang*, 1999; *Thompson and Wallace*, 2000].

[3] Many studies have analyzed the relationship between the SAM and climate variability in the SH. *Van den Broeke and Van Lipzig* [2002] indicated that the anomaly of SAM may change the winter tropospheric vertical and meridional circulation and consequently surface air temperature in the East Antarctica. *Genthon et al.* [2003] found the SAM signal in Antarctic precipitation anomalies. The SAM also may influence precipitation over southeastern South America because of the atmospheric circulation [*Silvestri and Vera*, 2003].

[4] The SAM variability not only has relation to the climate systems at midlatitude–high latitudes of the SH [e.g., *Reason and Rouault*, 2005; *England et al.*, 2006; *Ummenhofer et al.*, 2008], but also the climate in the Northern Hemisphere (NH). Studies [*Nan and Li*, 2003; *Gao et al.*, 2003] found that strong positive SAM events in spring are followed by weak East Asian summer monsoon (EASM); and vice versa. The interaction between sea surface temperature (SST) in the Indian Ocean (IO) and Asian summer monsoon has been examined extensively. Numerical models indicated that the variability of Asian summer monsoon is sensitive to the conditions of SST in the tropical southern IO [*Zhu and Houghton*, 1996]. *Terray et al.* [2003] pointed out that strong (weak) Indian summer monsoons are preceded by significant positive (negative)

[1]Chinese Academy of Meteorological Sciences, Beijing, China.
[2]Laboratory for Climate Studies, China Meteorological Administration, Beijing, China.
[3]National Key Laboratory of Numerical Modeling for Atmospheric Sciences and Geophysical Fluid Dynamics, Institute of Atmospheric Physics, Chinese Academy of Sciences, Beijing, China.
[4]Lamont-Doherty Earth Observatory, Columbia University, Palisades, New York, USA.

0148-0227/09/2008JD010045$09.00

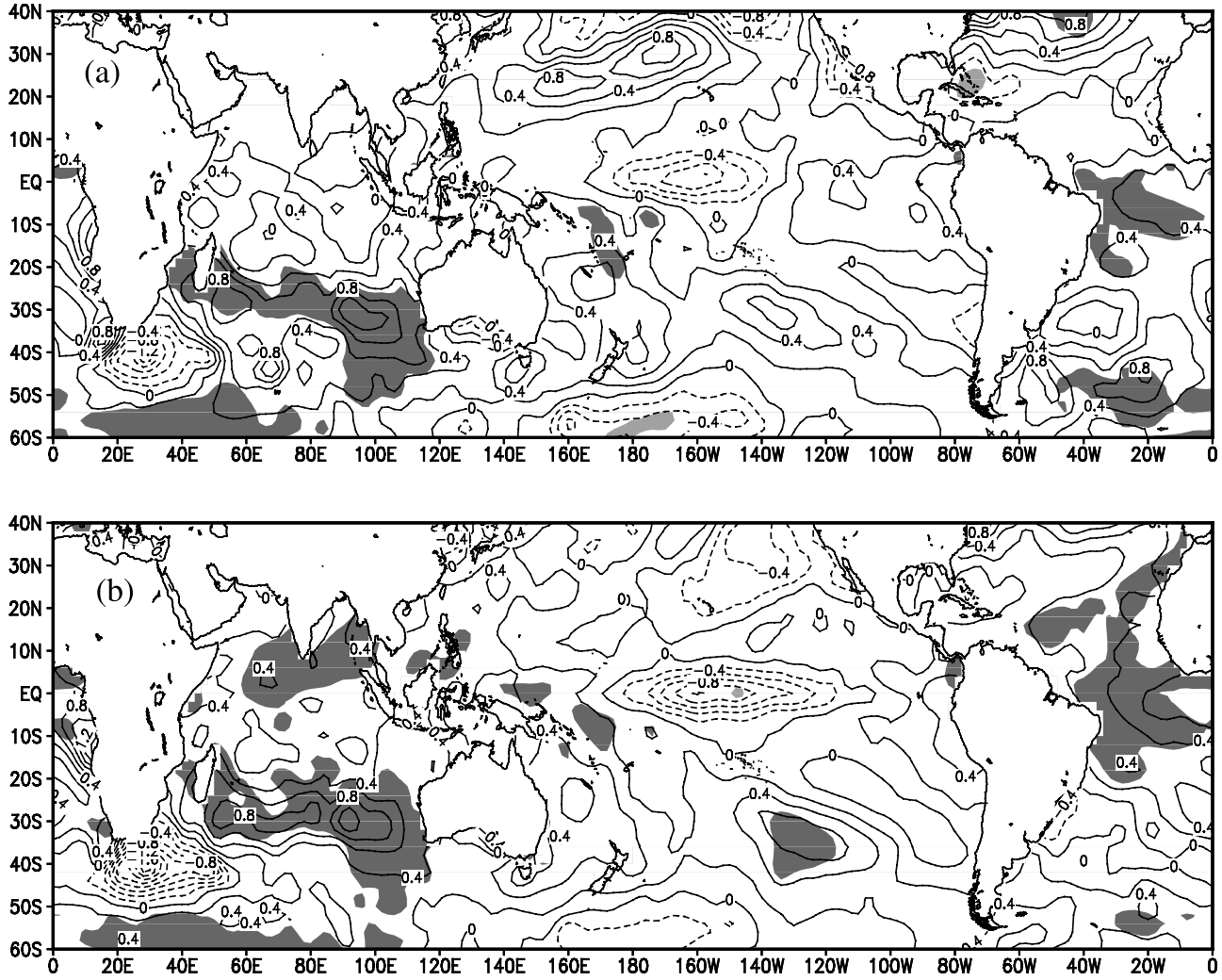

Figure 1. Composite differences in SST (°C) between the high and low spring (April–May) SAMI cases in (a) spring (April–May) and (b) summer (June–August). The dark and light shaded areas are significant at the 99% confidence level for positive and negative differences, respectively. The counter interval is 0.2°C.

SST anomalies in the southeastern subtropical IO during boreal winter. *Terray et al.* [2005] further emphasized the importance of the southern IO for an ENSO-monsoon relationship. *Kucharski et al.* [2006] recently documented that in decadal timescale, cold (warm) Indian equatorial SST causes low-level divergence (convergence) that in turn modifies the local Hadley circulation and strengthens (weakens) the Indian monsoon circulation. These studies all indicate that the IO SST plays an important role in the variability of the Asian monsoon.

[5] The physical processes that link the IO SST variability to atmospheric forcing have also been investigated. *Klein et al.* [1999] pointed out that the warming of the IO surface may have been partly a response to remote forcing from the Pacific. During El Niño events, an anomalously warm SST in the central-eastern Pacific reduces cloud cover over the IO and allows in more solar radiation to warm the sea surface. *Reason et al.* [2000] demonstrated that the changes of wind in the IO affect SST through surface turbulent heat fluxes. *Fauchereau et al.* [2003] showed the dipole-like SST variability in the South Indian and South Atlantic oceans in January–March. *Hermes and Reason* [2005] further pointed out that latent heat fluxes, upwelling, and Ekman heat transports associated with SAM and a wave number 3 or 4 pattern contribute to the dipole-like SST variability. The interaction of southern midlatitude zonal winds and ocean was also verified in GCM simulations [*Watterson*, 2000].

[6] Current studies on the subject mainly focus on the tropical IO. This paper emphasizes the importance of SST over the subtropics and middle latitudes of the Southern IO. The relationship of the spring SAM and EASM is investigated by analyzing the role of the IO SST in this teleconnection.

[7] Data sets and methods of analysis used in this study are described in section 2. The relationships among the boreal spring SAM, the IO SST and EASM are documented in section 3. The connections among the SSTs in different regions of the IO are examined in section 4. In section 5, we investigate possible physical processes that are responsible for connecting SST anomalies over the subtropics and

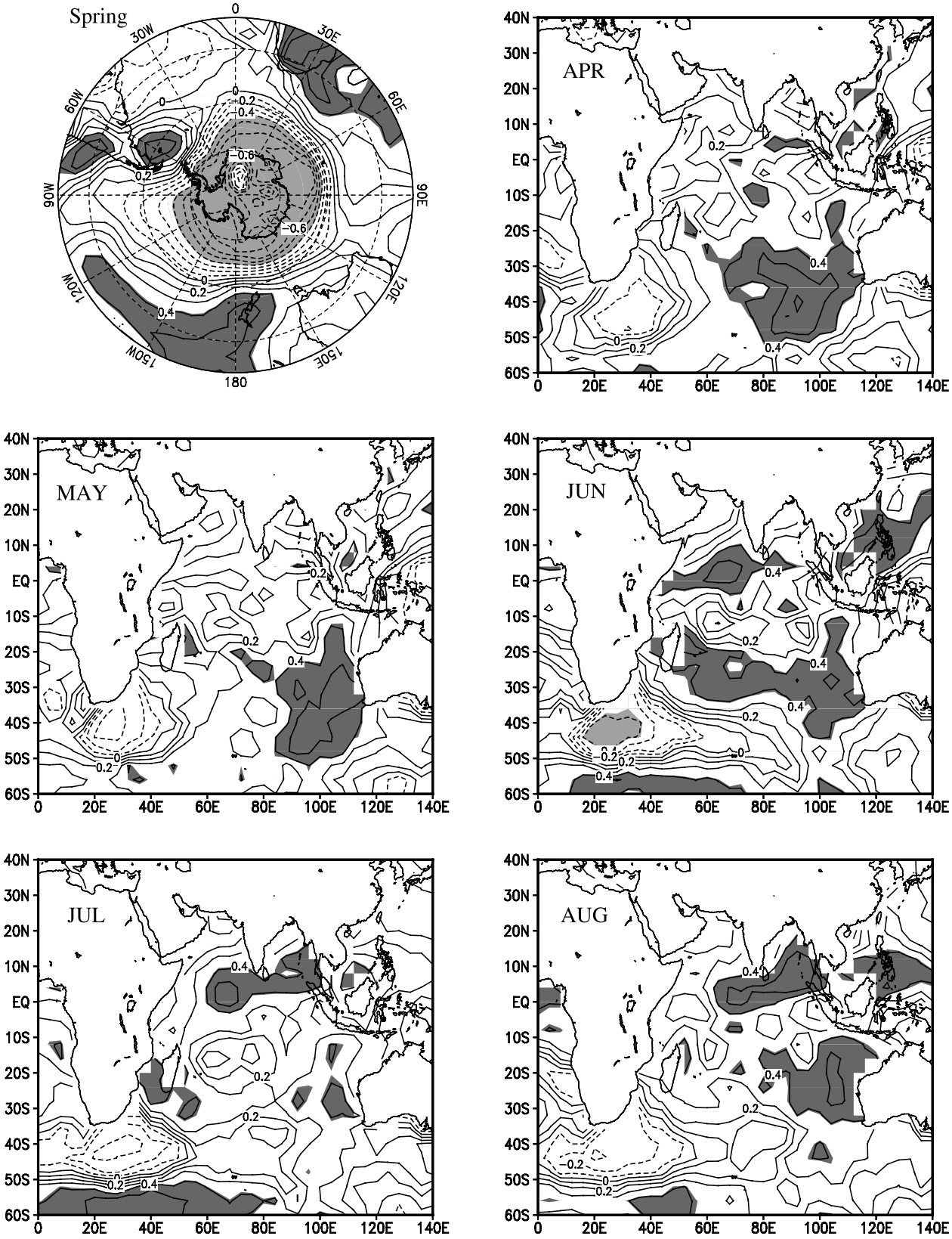

Figure 2. Heterogeneous correlation patterns of the leading ESVD mode for the spring (April–May) SH SLP anomalies south of 10°S (top left) and the Indian Ocean SST anomalies from April to August, respectively. The areas with positive (negative) correlation coefficients that are significant at the 99% confidence level are shaded dark (light). The latitude lines in the top left are at a 20-degree interval starting from 10°S.

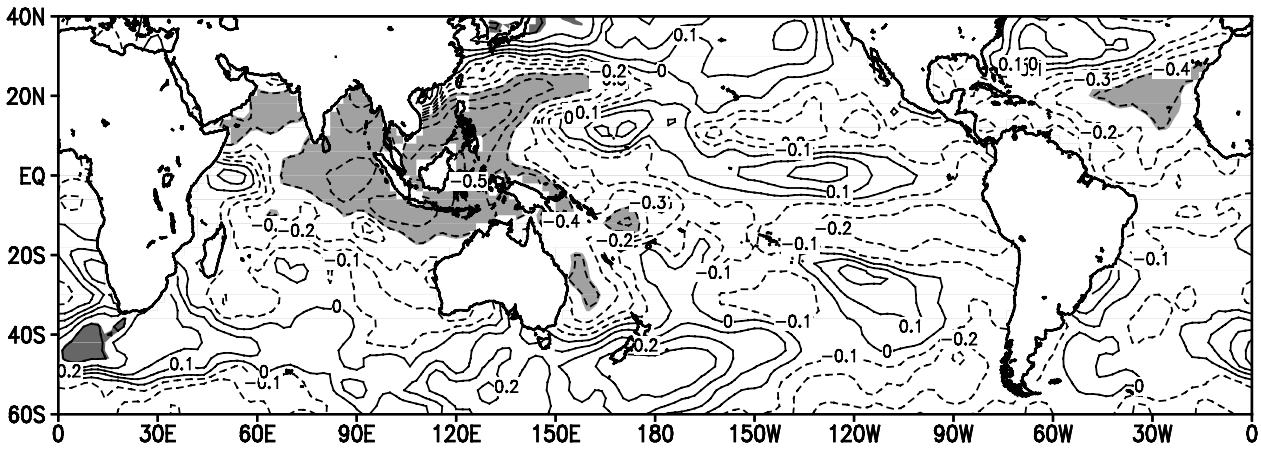

Figure 3. Correlation map between EASM index and SST in summer (June–August) for the period of 1958–2000. The positive (negative) correlation coefficients that are significant at the 99% confidence level are shaded dark (light). The contour interval is 0.1.

middle latitudes of the SIO and the spring SAM variability. On the basis of the above analyses, we summarize the role of the IO SST in the relationship between the boreal spring SAM and following EASM in section 6.

2. Data and Methods of Analysis

[8] We use several data sets in this study. Monthly mean SST data were obtained from National Climatic Data Center (NCDC) Extended Reconstructed Sea Surface Temperatures (ERSST) [*Smith and Reynolds*, 2004], with resolution of 2° latitude by 2° longitude covering 1958–2000. The SAM index (SAMI) (1958–2000) is the difference in the normalized zonal mean SLP (from NCEP-NCAR) between 40°S and 70°S [*Nan and Li*, 2003], which is a modification of the Antarctic Oscillation index defined by *Gong and Wang* [1999]. The East Asian summer monsoon (EASM) index is a unified monsoon index (dynamical normalized seasonality), which is given by

$$\delta = \frac{\|\overline{V}_1 - V_i\|}{\|\overline{V}\|} - 2$$

where $\overline{V}_1$, V_i are the January climatological and monthly wind vectors at a point, respectively, $\overline{V}$ is the mean of January and July climatological wind vectors at the same point. The norm $\|A\|$ is defined as $\|A\| = (\int\int s|A|^2\, dS)^{1/2}$, where s denotes the domain of integration (In calculations at a point (i, j), $\|A_{i,j}\| \approx \sqrt{a}((|A^2_{i-1,j}| + |A^2_{i,j}| + |A^2_{i+1,j}|)\cos\varphi_j + |A^2_{i,j-1}|\cos\varphi_{j-1} + |A^2_{i,j+1}|\cos\varphi_{j+1})^{1/2}$ where a is the mean radius of the earth and φ_j the latitude at the point (i, j)). The index nicely characterizes the seasonal cycle and interannual variability of monsoons for all known monsoon regions [*Li and Zeng*, 2002, 2003, 2005]. It is calculated by using the NCEP-NCAR reanalysis data for the period of 1958–2000. The SLP, sensible heat flux, latent heat flux, net longwave and solar radiation flux, and downward longwave and solar radiation flux for the period of 1958–2000 are from NCEP-NCAR reanalysis project [*Kalnay et al.*, 1996]. The quality of the flux data from the assimilation system are frequently questioned because they were created by using the prescribed SST. The comparison of monthly latent heat flux from NCEP-NCAR and the Goddard Satellite-Based surface Turbulent Fluxes version2 (GSSTF2) indicated that the differences in the latent heat flux between the two data sets are mainly in the tropical Pacific and the annual mean and temporal variability of the latent heat flux from NCEP-NCAR are close to those from GSSTF2 in most regions of the IO [see *Feng and Li*, 2006, Figures 3c and 3d]. *Yu et al.* [2007] evaluated surface net heat fluxes in the IO derived from six products (including the NCEP-NCAR reanalysis) on their annual, seasonal, and interannual variabilities. They found no major bias in the seasonal cycle of five products (including the NCEP-NCAR reanalysis) despite the fact that large differences in the mean of heat flux exist among the six products. They concluded that four products (including the NCEP-NCAR reanalysis) can be used for studying inter-

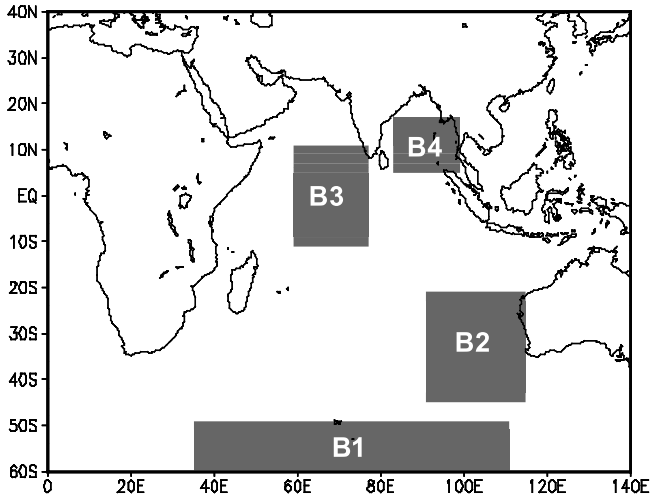

Figure 4. Oceanic region sites at middle latitudes of the South Indian Ocean (B1), to southwest of Australia (B2), in the equatorial Indian Ocean (B3), and in the Bay of Bengal (B4).

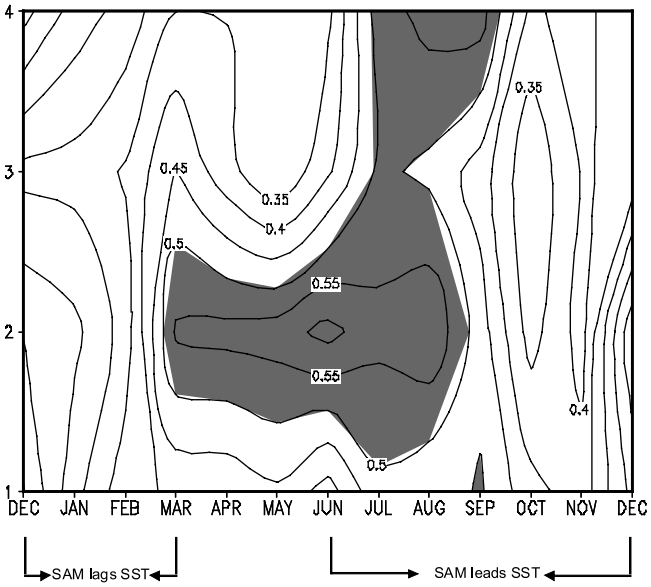

Figure 5. Lead-Lag correlations between the spring (April–May) SAMI and SSTs in B1, B2, B3, and B4, represented by 1–4 in the *y* axis from SAM lags 4 months to SAM leads 7 months. The correlation coefficients larger than 0.5 are shaded.

annual variability. Since other atmospheric variables used in this paper are from NCEP-NCAR, for example SLP and EASM index, we choose to use the flux data from NCEP-NCAR reanalysis for data coherence. The boreal spring and summer is defined as April–May and June–August, respectively.

[9] Following methods are applied in this study.

[10] 1. Composites

[11] The composite analysis is used to examine the variabilities of the IO SST associated with the extreme SAM events and corresponding physical processes. The high and low SAMI cases were selected based on the fluctuations of the index beyond one standard deviation. The high spring SAMI cases occur in 1976, 1989, 1993, 1995, 1996, 1998, 1999 and 2000, and the low spring SAMI cases occur in 1958, 1959, 1960, 1965, 1966, 1968, 1980 and 1990.

[12] 2. ESVD (extended singular value decomposition)

[13] Singular Value Decomposition is a technique of studying the pertinent fields of two variables. ESVD analysis is an extension of SVD and may extract a propagating phenomenon with time [*Kuroda and Kodera*, 2001]. In this paper, it is employed to examine the persistence of SST anomalies in the SIO and the appearance of SST anomalies in the equatorial Indian Ocean and Bay of Bengal in the following season.

[14] 3. Simultaneous correlation and lead-lag correlation

[15] The simultaneous correlation is employed to illustrate the relationship between the EASM and SST in the equatorial Indian Ocean and Bay of Bengal. The lead-lag correlations are applied to examine the potential casual relationships between boreal spring SAM and SST anomalies over the subtropics and middle latitudes of the SIO as well as SST anomalies in the equatorial Indian Ocean and Bay of Bengal.

[16] The Student's *t* test is used to assess the statistical significance of the results obtained from composite and correlation analyses unless specified.

3. Relationships Among the Boreal Spring SAM, the IO SST, and EASM

[17] Figure 1a presents the composite differences of simultaneous SST anomalies between the high and low spring SAMI cases. The significant positive values cover the midlatitude oceanic regions over 50°S–60°S and the subtropics at 20°S–35°S. There is no significant anomaly in the tropical Indian Ocean. In summer (Figure 1b), large-scale significant positive SST anomalies appear in the equatorial Indian Ocean and Bay of Bengal. The SST anomalies in the tropical Indian Ocean strengthen from spring to summer and the spring positive SST anomalies over the subtropics and middle latitudes of the SIO persist to the following summer. As well known, the warming trend in the IO and the positive trend in SAM are significant in the recent decades [*Bader and Latif*, 2003; *Hoerling et al.*, 2004; *Thompson et al.*, 2000]. To isolate the contribution of the trends from that of natural variability, we removed both the trends of SAM and SST, and recalculated the composite differences of detrended SST anomalies between the high and low detrended spring SAMI cases (figures are not

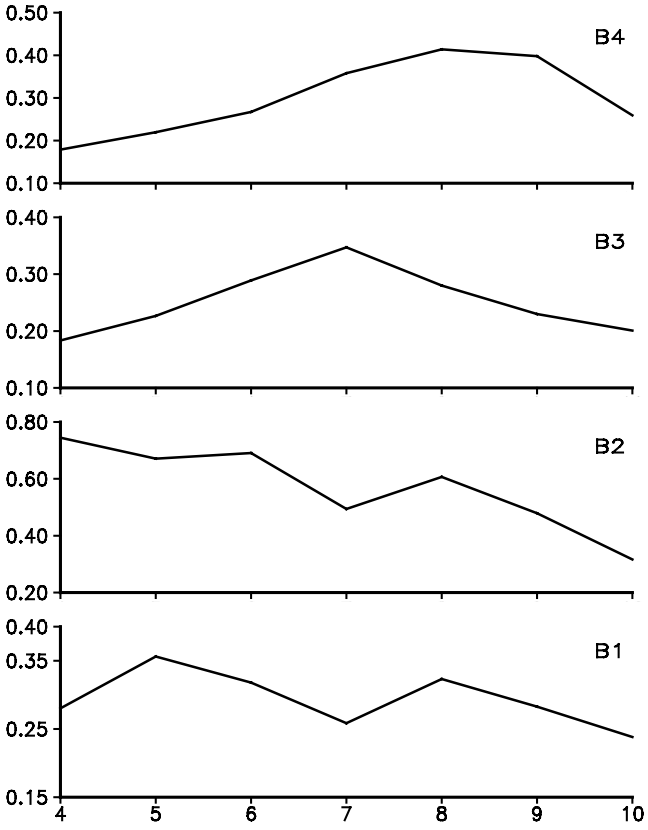

Figure 6. Composite differences of SSTs in B1, B2, B3, and B4 (from the bottom to top) from April to October between the high and low spring SAMI cases.

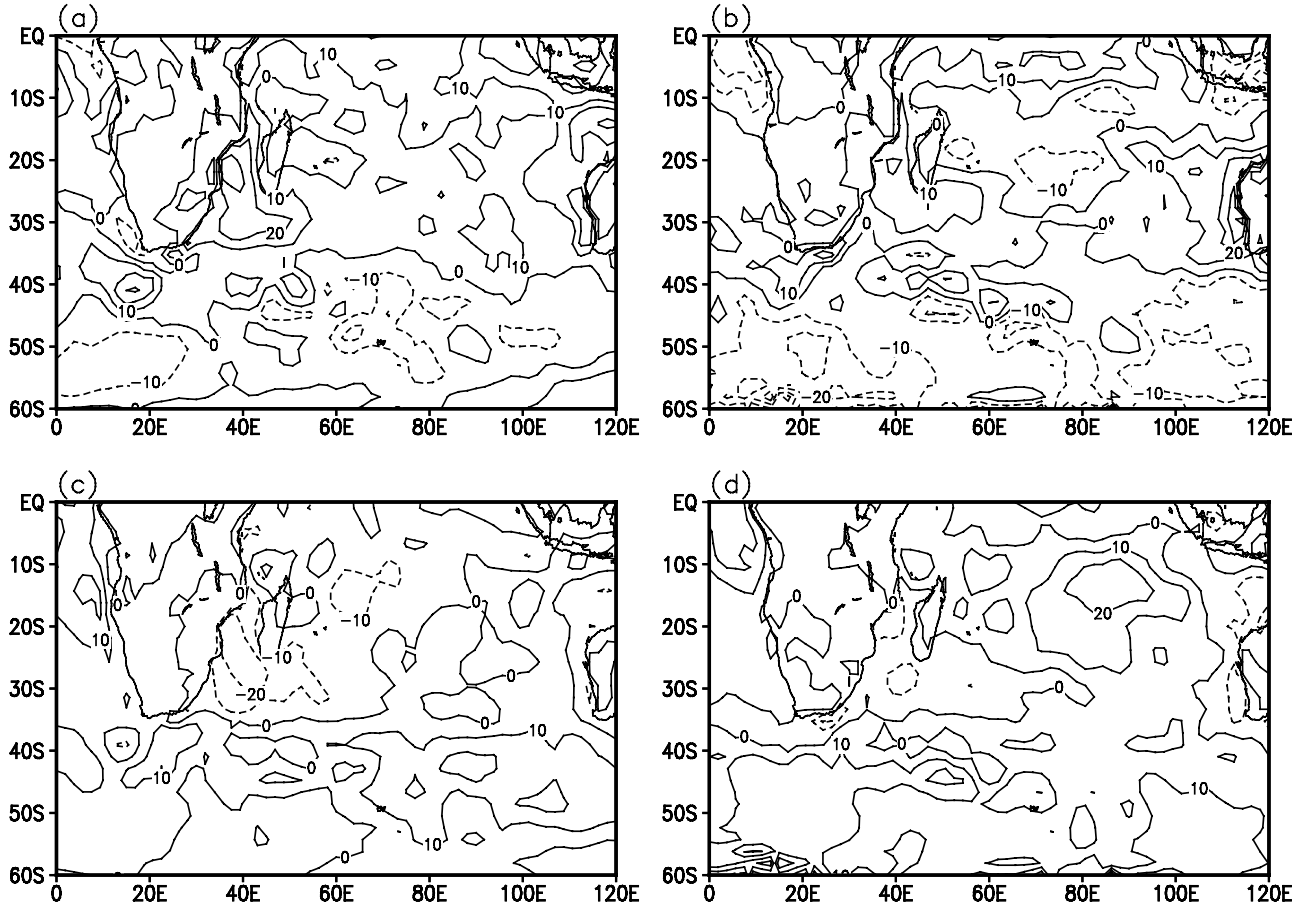

Figure 7. Composites of total net surface heat flux anomaly (W m^{-2}) (including the sensible heat flux, latent heat flux, net longwave flux, and solar radiation flux) in the Indian Ocean in (a, c) spring and (b, d) summer for the high spring SAMI cases in Figures 7a and 7b and low spring SAMI cases in Figures 7c and 7d.

shown). After removing the linear trends, the eight highest SAMI years occur in 1961, 1962, 1964, 1976, 1979, 1989, 1995 and 1999, and the eight lowest SAMI years in 1965, 1966, 1968, 1980, 1981, 1986, 1990 and 1992. The general patterns of SST anomalies remain the same: significantly positive SST anomalies in spring occur over the subtropics and middle latitudes of the SIO, which persist to summer, followed by the significant positive SST anomalies in the equatorial Indian Ocean and Bay of Bengal in summer. Although after removing the linear trend, the regions with significant SST anomalies are reduced comparing to those based on the original SAMI and SST time series, the sequence of SST anomaly developments in the IO remains the same. Therefore both linear trends and variabilities at other timescales contribute to the connection between SAM and IO SST anomalies.

[18] The variability of SST over the equatorial Pacific is the strongest signal of interannual climate variability and exerts important impacts on the climate and environment worldwide. We also see that negative SST anomalies in the equatorial central-eastern Pacific appear in the SST composite for strong positive phase of SAM in Figure 1. To sort out the relationships among SAM, ENSO and IO SST, we performed a conditional composite analysis, which selects the years with extreme events of spring SAM (larger than 0.5 standard deviation of the normalized SAMI) and the near-average spring equatorial Pacific SST (less than 0.3 standard deviation of the normalized values of Niño 3.4 SST (5°S–5°N, 170°W–120°W)). The high SAMI and near-average equatorial Pacific SST conditions occur in 1979 and 1996, while the low SAMI and near-average equatorial Pacific SST conditions occur in 1959 and 1960. In the composite differences of SST between the two sets of samples (figures are not shown), there is no significant ENSO SST pattern in the equatorial Pacific, but there are significant positive SST anomalies, similar to the patterns in Figure 1, occurring in the IO. That is, with near-average equatorial Pacific SST, IO SST still responds to the extreme spring SAM events. However, ENSO teleconnection to southern high latitudes has been well documented [*Yuan and Martinson*, 2001; *Liu et al.*, 2002]. Recent studies [*Zhou and Yu*, 2004; *Yuan and Li*, 2008] showed that ENSO and SAM share large amounts of variance at interannual timescale, which influences sea ice and SST variability in the Antarctic. Therefore the interaction among ENSO, SAM and the IO SST needs to be further examined in the future. SAM as a midlatitude–high latitude mode likely has a direct and independent relation with the IO SST variability.

[19] To further isolate the development of SST anomalies in the IO that are associated with the spring SAM variabil-

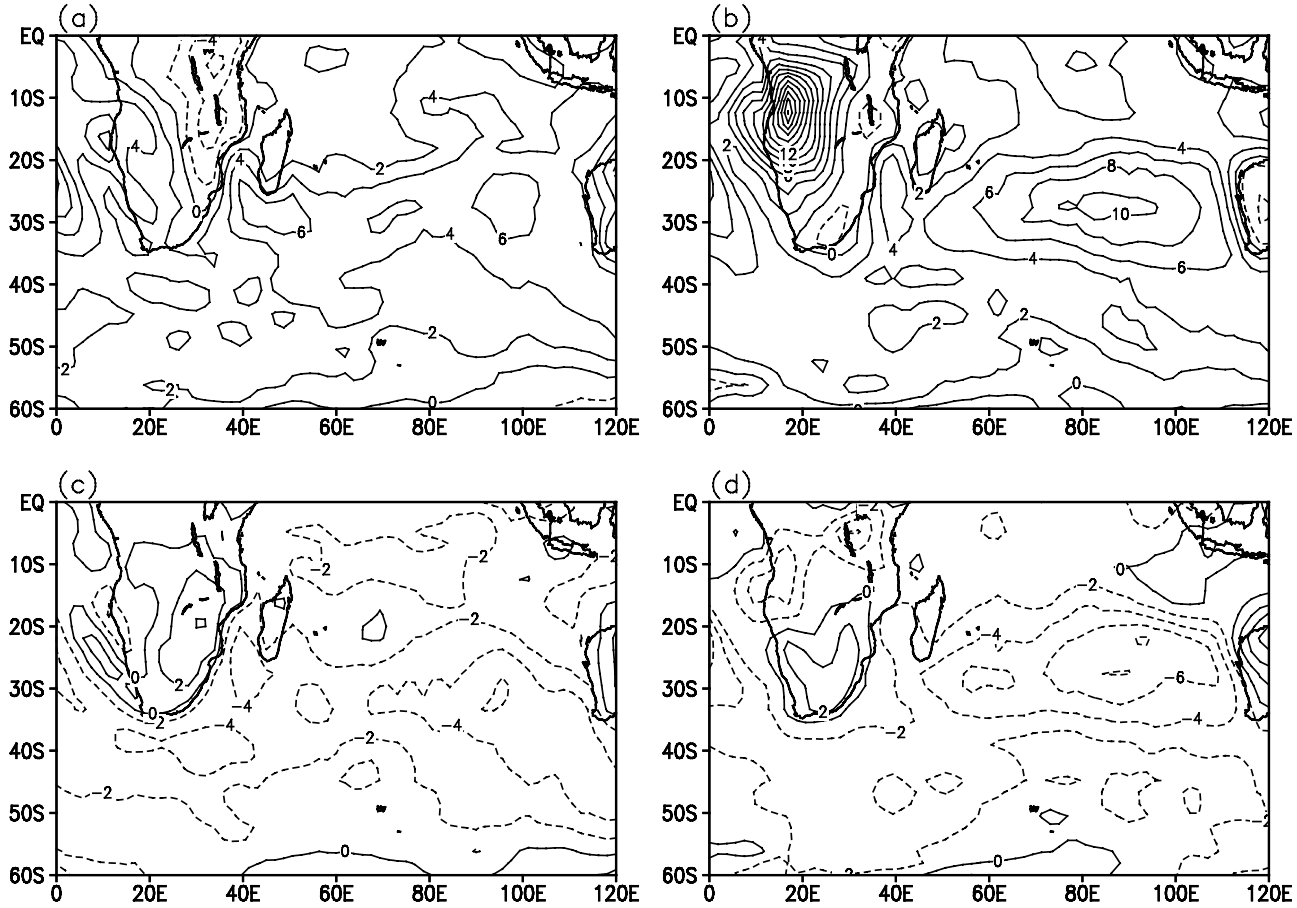

Figure 8. Same as Figure 7 except for the anomaly of downward longwave radiation flux (W m^{-2}).

ity, ESVD is applied to the extratropical SH SLP anomaly in spring and SST anomaly in the IO from April to August. Figure 2 illustrates the leading mode, which accounts for 60% of the total covariance between the boreal spring SLP anomalies and the combined 5-month SST anomalies. The first pattern of the extratropical SH SLP accounts for 21% of its total squared covariance and the first patterns of SST in the IO account for 19.5%, 20.4%, 22.8%, 21.2% and 19.8% of their total squared covariance from April to August, respectively. The extratropical SH SLP is characterized by the feature of the positive phase of SAM with significant negative correlation over southern polar cap and significant positive correlation over SH middle latitudes. For the SST field, in April–May, significant positive values are mainly over the subtropics and middle latitudes of the SIO and only a small region has significant positive correlation in the tropical Indian Ocean. In June, the SST anomaly pattern in the IO changes obviously: it shows the zonal belt feature and the correlation center over the subtropics and middle latitudes the SIO moves northward. It is more important that the significant correlation region in the equatorial Indian Ocean is expanded and the correlation center value increases from 0.4 in May to 0.5 in June. In July–August, the significant correlation region further extends to Bay of Bengal. In summary, when the spring SAM is in its strong positive phase, positive SST anomalies occur over the subtropics and middle latitudes of the SIO, which are followed by the increased SST in the equatorial Indian Ocean and Bay of Bengal in summer.

[20] The above analyses endorse the hypothesis that the spring SAM events are connected with the SST anomalies over the subtropics and middle latitudes of the SIO and followed by the summertime SST anomalies in the equatorial Indian Ocean and Bay of Bengal. An early study [*Nan and Li*, 2003] has suggested that the strong positive phase of the spring SAM is followed by the weakened EASM, and vice versa. Here we show that EASM variability is also related to SST anomalies in the equatorial Indian Ocean and Bay of Bengal. Figure 3 presents the correlation map between the EASM index and the IO SST in summer. The equatorial Indian Ocean, Bay of Bengal and South China Sea are covered by significant negative correlations, indicating that the weakened EASM is associated with the warmed SST in the these regions; and vice versa. EASM comes through a weakening process and showed an apparent trend in the recent decades [*Chen et al.*, 1992]. We removed both the trends of the EASM index and SST and recalculated the correlation between them (figure is not shown). The resulting correlations show the same patterns as before, although the regions with significant correlation are reduced. Therefore both linear trends and variabilities at other timescales contribute to the connection between EASM and SST anomalies in the equatorial Indian Ocean, Bay of Bengal and South China Sea.

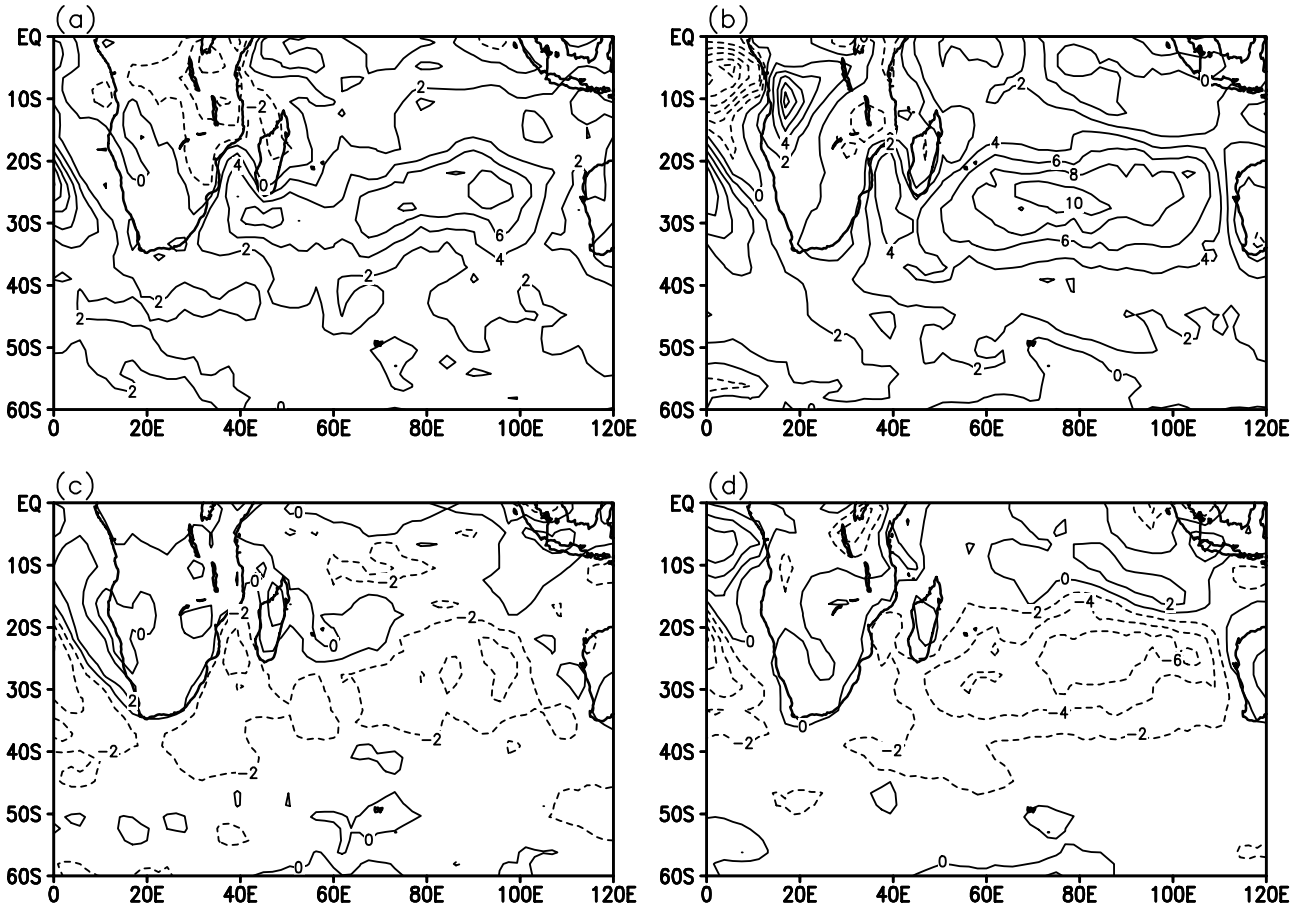

Figure 9. Same as Figure 7 except for the anomaly of low cloud cover (%).

[21] In summary, when the spring SAM is strong positive, large-region positive anomalies of SST occur over the subtropics and middle latitudes of the SIO, which persist from spring to summer. Meanwhile, a small area of positive SST anomalies exists in the tropical Indian Ocean, which is enhanced and expanded from spring to summer. The increased SST in the SIO associated with the strong positive SAM in spring seems to be followed by the increased SST in the equatorial Indian Ocean and Bay of Bengal in summer. Furthermore, EASM is closely related to SST in the equatorial Indian Ocean, Bay of Bengal and South China Sea. When SST in these regions is above near average, EASM tends to be weak. Therefore the IO SST is associated with SAM and EASM, which plays an important bridging role in the SAM-EASM relationship.

4. Connections Among the SSTs in Different Regions of the IO

[22] As presented above, SST anomalies in the IO are associated with SAM variability in boreal spring and EASM in the following season. Here we examine how these associated IO SST anomalies are established and how they evolve through these two seasons.

[23] For the convenience of the study, the IO is partitioned into four regions (Figure 4) based on the distribution of SST anomalies associated with the spring SAM (as shown in Figure 1). The oceanic region at middle latitudes of the SIO is defined as the area of 36°E to 110°E in longitudes and 50°S to 60°S in latitudes (B1); the region to the southwest of Australia is from 92°E to 114°E in longitudes and 22°S to 44°S in latitudes (B2); the equatorial Indian Ocean region is from 60°E to 76°E in longitudes and 10°S to 10°N in latitudes (B3); Bay of Bengal region is from 84°E to 98°E in longitudes and 6°N to 16°N in latitudes (B4). Each regional mean SST is used to represent the SST variability in the whole region.

[24] Figure 5 shows the correlations between the spring SAMI and the SSTs in the four oceanic regions from SAM lags 4 months to SAM leads 7 months. The lagged correlation coefficients (SAM lags SSTs) are much weaker than the leading correlation coefficients (SAM leads SSTs). In other words, the correlation coefficients are stronger when the SSTs in these four oceanic regions lag spring SAM events, suggesting that the primary process is the atmosphere forcing the ocean, instead of the ocean forcing the atmosphere. The high correlation coefficients in B1 and B2 begin in March–May, then persist into June–August. These high correlation coefficients spread to B3 and B4 in July and persist through September in these regions. This reveals that not only the SST anomalies in B1–B2 were a strong persistence trait, but also the SST anomalies in B3–B4 follow those in B1–B2 and persist through the summer too.

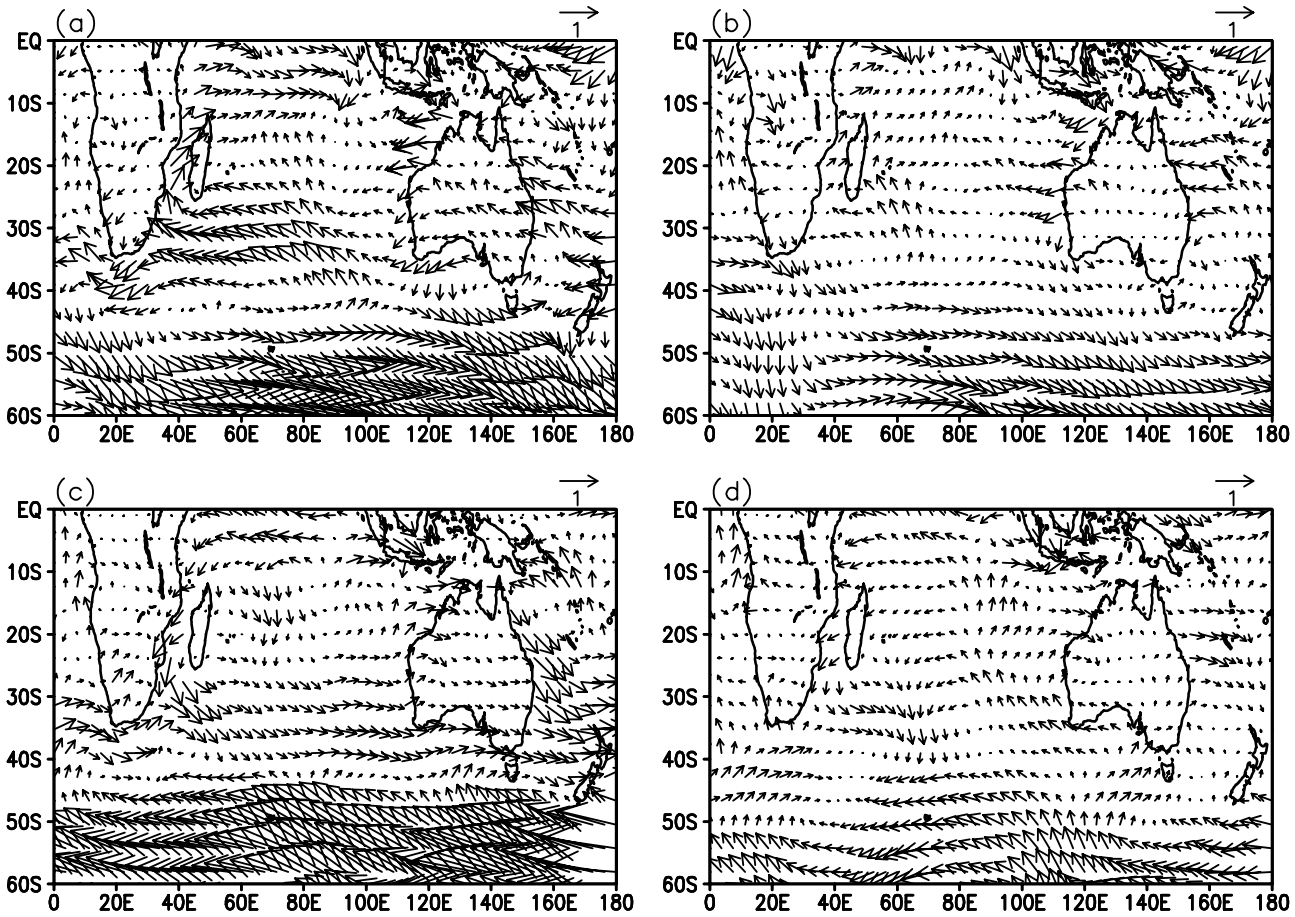

Figure 10. The composites of surface wind anomaly (m s^{-1}) vectors in (a, c) spring and (b, d) summer for the high spring SAMI cases in Figures 10a and 10b and low spring SAMI cases in Figures 10c and 10d.

[25] During the 43-a period from 1958 to 2000, the numbers of years during which the SAMI anomaly sign is same as the SST anomaly signs in the spring are 27, 31, 26 and 25 in B1, B2, B3 and B4, account for 62.8%, 72.1%, 60.4% and 58.1% of the total number of years, respectively. The numbers of years during which the sign of spring SAMI anomaly is same as the sign of summer SST anomaly are 31, 35, 29 and 27, respectively, account for 72.1%, 81.4%, 67.4% and 62.8% of the total number of years. These statistics show that following the strong positive (negative) spring SAM events, the SSTs in the four oceanic regions tend to be warmer (colder) than normal in the same season and the following summer. The numbers of years during which the SST anomaly signs are consistent in spring and summer are 33, 33, 34 and 35, respectively, account for 76.7%, 76.7%, 79.1% and 81.2% of the total number of years. It also suggests that the SST anomalies in all these regions have a strong persistence from spring to summer.

[26] Figure 6 is the composite difference of SST anomalies in the four oceanic regions between the high and low spring SAMI cases from April to October. The highest anomalies in B1 and B2 are concentrated in April–May and the highest anomalies in B3 and B4 are in July–August. These further verified the above finding that the spring SAM events has close relation to SST anomalies over the subtropics and middle latitudes, which is followed by the SST anomalies in the equatorial Indian Ocean and Bay of Bengal.

5. Possible Physical Processes Responsible for the SST Anomaly in the SIO

[27] The above analyses show SST anomalies in the SIO are associated with SAM variability. To examine potential physical processes responsible for the relationship, heat fluxes at the air-sea interface and atmospheric circulations in the SIO are analyzed.

[28] Changes in the oceanic heat budget and transport are of great importance for the understanding of global climate. In climatology, the ocean releases heat to the atmosphere in the IO in boreal spring and summer. Figure 7 shows the composites of total net surface heat flux (including sensible heat flux, latent heat flux, net longwave and solar radiation flux) anomalies for the high and low spring SAMI cases. For the net flux from NCEP-NCAR data, positive values mean that the ocean vents the heat to the atmosphere. For the high (low) SAMI cases, the anomalies of net surface heat flux are negative (positive) at about 50°S–60°S in spring and summer, indicating that ocean releases less (more) net heat to the atmosphere, which is consistent with

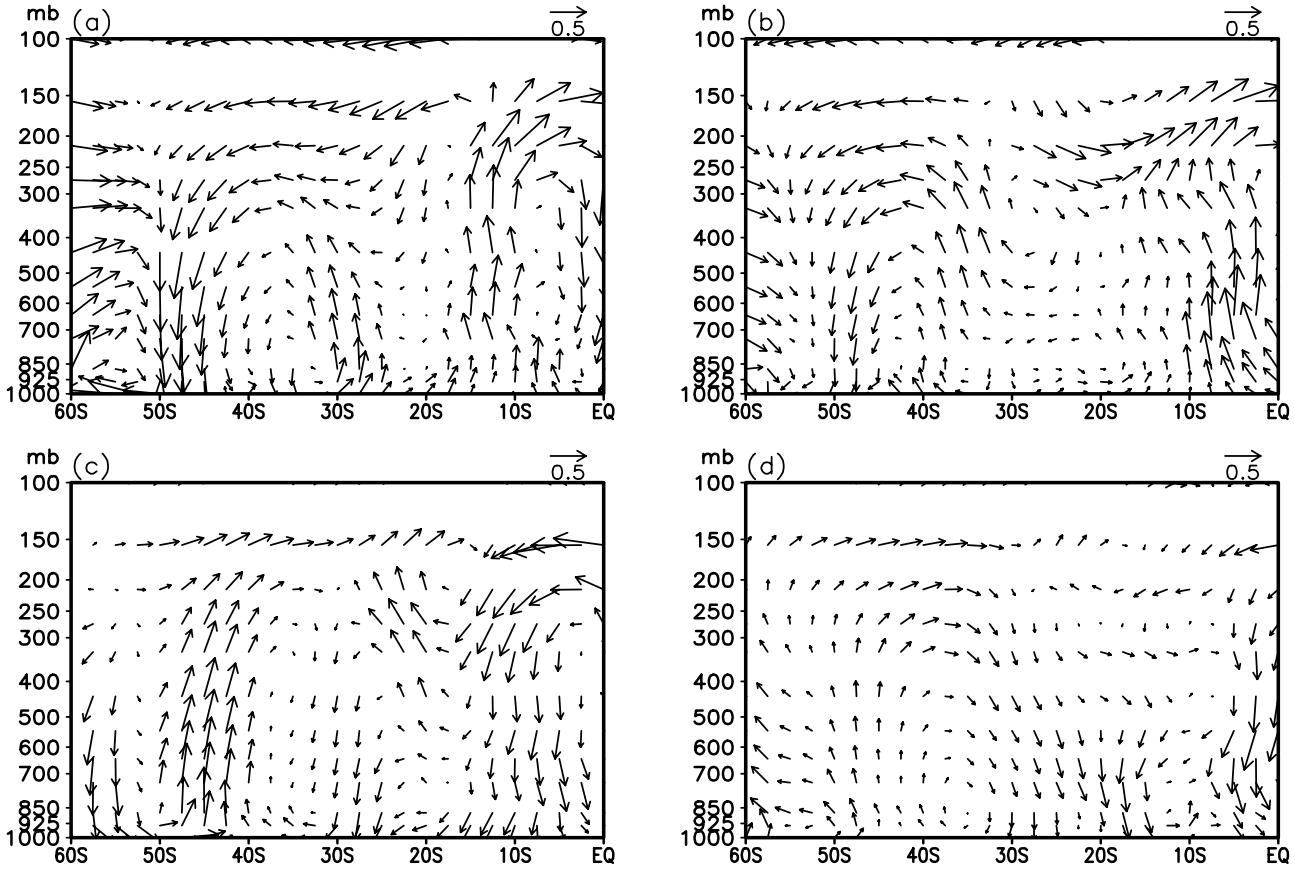

Figure 11. The latitude-pressure cross sections of meridional (m s^{-1}) and vertical wind anomaly (Pa s^{-1} * 100) vectors averaged between 20°E and 120°E in (a, c) spring and (b, d) summer for the high spring SAMI cases in Figures 11a and 11b and low spring SAMI cases in Figures 11c and 11d.

the increase (decrease) of SST. Therefore the SST anomalies at 50°S–60°S of the SIO are likely a result of responding to the change in surface heat flux.

[29] Then, we examined the anomalies of each component of total net surface heat flux to isolate the dominant contributor to the SST anomalies in the SIO. Among them, the longwave radiation flux seems to have such a connection. The change of the net longwave radiation flux coincides with the SST anomalies over the subtropics of the SIO. It reflects the downward longwave radiation flux (Figure 8). For the high SAMI cases, positive anomalies of downward longwave radiation flux are centered at 20°S–30°S with maximum of 6 W m^{-2} in spring and 10 W m^{-2} in summer, indicating the increase of the downward longwave radiation flux (Figures 8a and 8b). The increased downward longwave radiation warms the sea surface. For the strong negative SAMI cases, the negative anomalies of the downward longwave radiation occur in the SIO, which are centered near 30°S with the maximum magnitude of ~6 W m^{-2} in spring and ~8 W m^{-2} in summer. It suggests the decrease of downward longwave radiation flux, in favor of the decrease of SST (Figures 8c and 8d). The anomalies of downward longwave radiation flux match the SST anomalies over the subtropics in Figure 1, suggesting its dominant contribution to the change in SST.

[30] The cloud cover is an important factor influencing the magnitude of the downward longwave radiation flux. Figure 9 shows the composites of low cloud cover anomalies for the high and low SAMI cases. For the high SAMI cases, positive anomalies appear in the SIO near 20°S–30°S with a maximum magnitude of 8% in spring and 10% in summer, indicating the increase of low cloud cover. That is consistent with the increase of the downward longwave radiation flux in Figures 8a and 8b. For the low SAMI cases, negative anomalies occur over the subtropics of the SIO with centers near 20°S–30°S. The magnitudes in these centers are −4% in spring and −6% in summer, indicating the decrease of the low cloud cover. The cloud may absorb and reflect the solar radiation, and cool the Earth surface. It may also absorb and emit the longwave radiation, and warm the Earth surface. The distributions of anomalies of the low cloud cover and downward longwave radiation flux are matched nicely in Figures 8 and 9, suggesting the anomalies of the low cloud cover might be the cause of the change of downward longwave radiation flux. The anomalies of downward longwave radiation are also collocated with SST anomalies in Figure 1. Therefore the low cloud may play a role in warming the sea surface in the subtropics of the SIO through changing the downward longwave radiation.

[31] How does spring SAM influence the low cloud cover over the subtropics of the SIO? Figure 10 is composites of the surface wind anomaly vectors for the high and low SAMI cases. When SAM is in its strong positive phase,

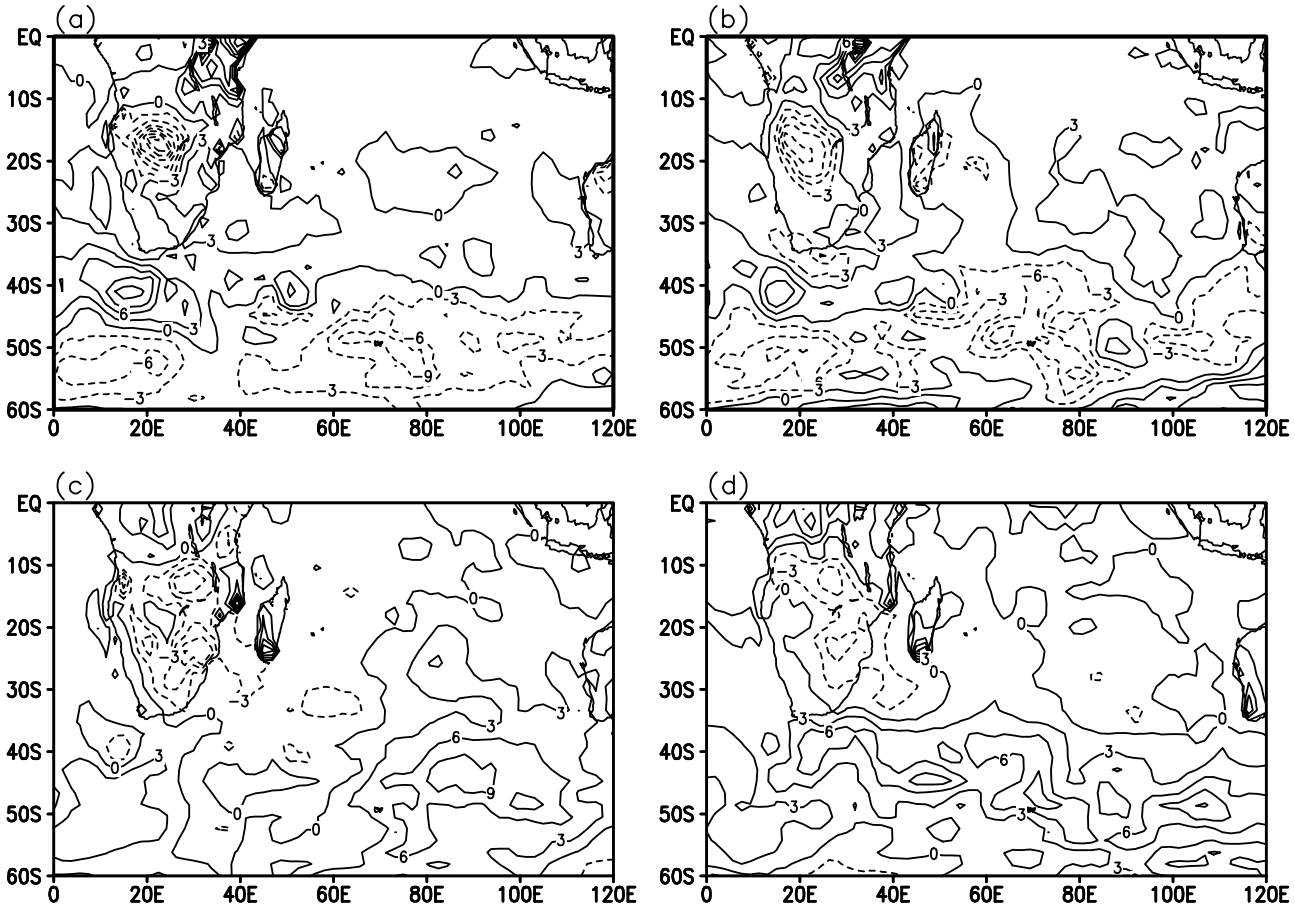

Figure 12. Same as Figure 7 except for the anomaly of sensible heat flux (W m^{-2}).

subtropical highs move southward. An anomalous anticyclone appears to the southeast of Africa near 40°S–50°S and an anomalous cyclone occurs in the eastern SIO near 20°S–30°S (Figure 10a). Accordingly, anomalous upward motions prevail in the middle–lower troposphere at 20°S–30°S, and anomalous downward motions at 40°S–50°S (Figure 11a), indicating that the regional Ferrel Cell weakens. The large-scale anomalous upward motions may cause the increase of low cloud cover and downward longwave radiation flux. When SAM is in its strong negative phase, a pair of anomalous cyclone and anticyclone dominates the region to the southeast of Africa and the eastern IO, and the regional Ferrel Cell strengthens (Figures 10c and 11c). The anomalous downward motions (Figure 11c) at 20°S–30°S reduce the low cloud cover and then the downward longwave radiation flux. In summer, the surface wind fields and vertical circulations are not completely symmetrical for the high and low SAMI cases. For the low SAMI cases, the horizontal and vertical circulations keep the features in spring (Figures 10d and 11d). For the high SAMI cases, the anomalous cyclone in the eastern SIO in spring is not apparent in summer (Figure 10b). However, it is noticed that anomalous upward motions occur in large regions at 10°S–40°S (Figure 11b). Moreover, the surface circulations are completely different at middle-lower latitudes for the high and low SAMI cases. Therefore SAM variability does change the summer atmospheric circulations at 20°S–40°S. The change of atmospheric circulations associated with SAM causes the anomalies of low cloud cover and downward longwave radiation, and then leads to the SST anomalies over the subtropics of the SIO.

[32] The change in sensible heat flux is partly responsible for SST anomalies in the midlatitudes of SIO at 50°S–60°S. For the high SAMI cases, negative anomalies of the sensible heat flux cover the middle latitudes at 50°S–60°S in spring and summer (Figures 12a and 12b), indicating the reduced sensible heat flux from the ocean to atmosphere. For the low SAMI cases, reversed anomalies appear in the middle latitudes of the SIO at 50°S–60°S, indicating the increased sensible heat flux from the ocean to atmosphere (Figures 12c and 12d). The completely different sensible heat flux changes for the high and low SAMI cases imply that the SAM variability does change the sensible heat flux in middle latitudes of the SIO at 50°S–60°S. The reduced (enhanced) sensible heat fluxes are in favor of the increase (decrease) of SST.

[33] During the strong positive SAM phase, the anomalous surface atmospheric circulation shows northerly winds to the south of South Africa and Australia at 40°S–60°S (Figures 10a and 10b), which could transport more (less) warmer (colder) air from middle latitudes north of 50°S (high latitudes) into 50°S–60°S and warm the air. The warmed air at 50°S–60°S reduces the temperature difference between the ocean and atmosphere and thus reduces the sensible heat flux from the ocean to atmosphere, resulting in positive SST anomalies. The westerly winds

strengthen at 50°S–60°S (Figure 10a). However, the increased wind speed isn't consistent with the decrease of the sensible heat flux. Therefore the reduced sensible heat flux is due to warm air advection instead of increased wind speed. During the strong negative SAM phase, anomalous southerly winds appear at 40°S–60°S and more (less) colder (warmer) air from high latitudes (middle latitudes, north of 50°S) comes into 50°S–60°S and cools the air in the region (Figures 10c and 10d). The temperature difference between the ocean and atmosphere increases, leading to the enhanced sensible heat flux from the ocean to atmosphere.

[34] It is hypothesized that the positive subtropical ridge anomalies around 40°S due to the strong SAM may allow more solar radiation in the ocean surface. However, it is not verified in observation. In the composites of downward solar radiation fluxes for the high spring SAMI cases (figures are not shown), downward solar radiation fluxes are reduced over the subtropics and middle latitudes of the SIO south of 20°S for high SAMI cases, which is not consistent with the increase of the local SST.

6. Conclusion and Discussion

[35] Using the monthly means from the NCEP-NCAR reanalysis and ERSST data sets for the period of 1958–2000, we investigated the relationships among boreal spring SAM, IO SST and EASM. We found that the variability of IO SST is significantly correlated with the spring SAM events and EASM. When the spring SAM is strong positive, SST over the subtropics and middle latitudes of the SIO increases, which is followed by the increased SST in the equatorial Indian Ocean and Bay of Bengal in summer. The increased SST in the equatorial Indian Ocean and Bay of Bengal is associated with the weak EASM. Therefore the IO SST plays an important bridging role in the SAM-EASM relationship. SAM, IO SST and EASM all showed linear trends in the recent decades. Both linear trends and variabilities at other timescales contribute to the connections among them. If SAM continues to increase in the future and its relationships with IO SST anomalies and EASM hold, we would expect to see weaker EASM in the future. Although this SAM, IO SST and EASM teleconnection seems to covary with ENSO events in the tropical Pacific, it also exists without any tropical forcing. Under conditions of near-average SST over the equatorial central-eastern Pacific, the relationship between SAM extreme events and IO SST anomalies remains the same. This could suggest that SAM has independent relation to SST at lower latitudes of the IO, even though it shares significant amount of variance with ENSO in the tropical Pacific.

[36] The analyses of SAM and SSTs in the different regions of the IO further indicate that SAM is closely related with the IO SST anomalies, which may persist from spring to summer. And, the SST anomalies over the subtropics and middle latitudes of the SIO seem to be followed by the SST anomalies in the equatorial Indian Ocean and Bay of Bengal. Although the results are from simple statistical analyses, they suggest that the IO SST plays an important role in the SAM-EASM relationship.

[37] In this study, we investigate the physical processes that link the SAM variability with SST in the SIO. The changes in atmospheric circulations associated with SAM's variability and consequent changes in surface heat fluxes contribute to the SST variabilities in the SIO. When the spring SAM is in its strong positive phase, an anomalous anticyclone/cyclone pair appears to southeast of Africa and subtropical region of the eastern IO, respectively. The anomalous upward motions prevail in the eastern SIO and anomalous downward motions occur to the southeast of Africa, resulting in a weaker regional Ferrel Cell. The weakening of the downward branch of the Ferrel Cell causes the increase of the low cloud cover and then the downward longwave radiation flux. In addition, west of the anomalous anticyclone to the southeast of Africa, anomalous northerly winds transport more warm air into 50°S–60°S, which would reduce sensible heat fluxes and consequently generate SST anomalies. The increased downward longwave radiation and reduced sensible heat are likely responsible for the increase of SST in the SIO.

[38] In conclusion, it is air-sea interaction contributing to the relationships among the boreal spring SAM, IO SST and EASM. The variability of IO SST might play an important bridging role between the spring SAM and EASM. This paper presents a new pathway for the IO SST anomalies that may influence EASM.

[39] In spite of the simple explanations above, some physical processes are unclear. Through what processes do the SST anomalies in the equatorial Indian Ocean and Bay of Bengal connect with the SST anomalies in the SIO? Could the physical processes in this study be verified in numerical experiments? We only examine the heat exchange at the air-sea interface and the corresponding atmospheric circulation. Other possible processes in the ocean were not analyzed. In addition, this may be only one of many possible pathways that relate the spring SAM to EASM. These open questions need to be examined in the future.

[40] **Acknowledgments.** We thank the Climate Diagnostic Center/NOAA for providing the NCEP-NCAR reanalysis data and monthly mean ERSST data on its homepage. Three anonymous reviewers are thanked for the valuable comments on the manuscript. This work was jointly sponsored by the Chinese COPES project (GYHY200706005), 973 Program (2006CB403600), and the National Ocean and the Atmosphere Administration of USA through Grant NA030AR4320179.

References

Bader, J., and M. Latif (2003), The impact of decadal-scale Indian Ocean sea surface temperature anomalies on Sahelian rainfall and the North Atlantic Oscillation, *Geophys. Res. Lett.*, *30*(22), 2169, doi:10.1029/2003GL018426.

Chen, L., M. Dong, and Y. Shao (1992), The characteristics of interannual variations on the East Asian monsoon, *J. Meteorol. Soc. Jpn.*, *70*, 397–421.

England, M. H., C. C. Ummenhofer, and A. Santoso (2006), Interannual rainfall extremes over southwest Western Australia linked to Indian Ocean climate variability, *J. Clim.*, *19*, 1948–1969.

Fauchereau, N., S. Trzaska, Y. Richard, P. Roucou, and P. Camberlin (2003), Sea-surface temperature covariability in the southern Atlantic and Indian Oceans and its connect with the atmospheric circulation in the southern hemisphere, *Int. J. Climatol.*, *23*, 663–677.

Feng, L., and J. Li (2006), A comparison of latent heat fluxes over global oceans for ERA and NCEP with GSSTF2, *Geophys. Res. Lett.*, *33*, L03810, doi:10.1029/2005GL024677.

Gao, H., F. Xue, and H. Wang (2003), Influence of interannual variability of Antarctic oscillation on meiyu along the Yangtze and Huaihe River valley and its importance to prediction, *Chin. Sci. Bull.*, *48*, 61–67.

Genthon, C., G. Krinner, and M. Sacchettini (2003), Interannual Antarctic tropospheric circulation and precipitation variability, *Clim. Dyn.*, *21*, 298–307, doi:10.1007/s00382-003-0329-1.

Gong, D. Y., and S. W. Wang (1999), Definition of Antarctic oscillation index, *Geophys. Res. Lett.*, *26*, 459–462.
Hermes, J. C., and C. J. C. Reason (2005), Ocean model diagnosis of interannual coevolving SST variability in the South Indian and South Atlantic oceans, *J. Clim.*, *18*, 2864–2882.
Hoerling, M. P., J. W. Hurrell, T. Xu, G. T. Bates, and A. S. Phillips (2004), Twentieth century North Atlantic climate change. part II: Understanding the effect of Indian Ocean warming, *Clim. Dyn.*, *23*, 391–405, doi:10.1007/s00382-004-0433-x.
Kalnay, E., et al. (1996), The NCEP/NCAR 40-year reanalysis project, *Bull. Am. Meteorol. Soc.*, *77*, 437–471.
Kidson, J. W. (1975), Eigenvector analysis of monthly mean surface data, *Mon. Weather Rev.*, *103*, 182–186.
Klein, S. A., B. J. Soden, and N. C. Lau (1999), Remote sea surface temperature variations during ENSO: Evidence for a tropical atmospheric bridge, *J. Clim.*, *12*(4), 917–932.
Kucharski, F., F. Molteni, and J. H. Yoo (2006), SST forcing of decadal Indian monsoon rainfall variability, *Geophys. Res. Lett.*, *33*, L03709, doi:10.1029/2005GL025371.
Kuroda, Y., and K. Kodera (2001), Variability of the polar night jet in the Northern and Southern hemispheres, *J. Geophys. Res.*, *106*, 20,703–20,713.
Li, J. P., and Q. C. Zeng (2002), A unified monsoon index, *Geophys. Res. Lett.*, *29*(8), 1274, doi:10.1029/2001GL013874.
Li, J. P., and Q. C. Zeng (2003), A new monsoon index and the geographical distribution of the global monsoons, *Adv. Atmos. Sci.*, *20*, 299–302.
Li, J. P., and Q. C. Zeng (2005), A new monsoon index, its interannual variability and relation with monsoon precipitation (in Chinese), *Clim. Environ. Res.*, *10*(3), 351–365.
Liu, J., X. Yuan, D. Rind, and D. G. Martinson (2002), Mechanism study of the ENSO and southern high latitude climate teleconnections, *Geophys. Res. Lett.*, *29*(14), 1679, doi:10.1029/2002GL015143.
Nan, S. L., and J. P. Li (2003), The relationship between the summer precipitation in the Yangtze River valley and the boreal spring Southern Hemisphere Annular Mode, *Geophys. Res. Lett.*, *30*(24), 2266, doi:10.1029/2003GL018381.
Reason, C. J. C., and M. Rouault (2005), Links between the Antarctic Oscillation and winter rainfall over western South Africa, *Geophys. Res. Lett.*, *32*, L07705, doi:10.1029/2005GL022419.
Reason, C. J. C., R. J. Allan, J. A. Lindesay, and T. J. Ansell (2000), ENSO and climatic signals across the Indian Ocean Basin in the global context. part 1: Interannual composite patterns, *Int. J. Climatol.*, *20*, 1285–1327.
Rogers, J. R., and H. van Loon (1982), Spatial variability of sea level pressure and 500 mb height anomalies over the Southern Hemisphere, *Mon. Weather Rev.*, *110*, 1375–1392.
Silvestri, G. E., and C. S. Vera (2003), Antarctic oscillation signal on precipitation anomalies over southeastern South America, *Geophys. Res. Lett.*, *30*(21), 2115, doi:10.1029/2003GL018277.
Smith, T. M., and R. W. Reynolds (2004), Improved extended reconstruction of SST (1854–1997), *J. Clim.*, *17*(6), 2466–2477.
Terray, P., P. Delecluse, S. Labattu, and L. Terray (2003), Sea surface temperature associations with the late Indian summer monsoon, *Clim. Dyn.*, *21*, 593–618.
Terray, P., S. Dominiak, and P. Delecluse (2005), Role of the southern Indian Ocean in the transitions of the monsoon-ENSO system during recent decades, *Clim. Dyn.*, *24*, 169–195.
Thompson, D. W. J., and J. M. Wallace (2000), Annular modes in the extratropical circulation. part I: Month-to-month variability, *J. Clim.*, *13*, 1000–1016.
Thompson, D. W. J., J. M. Wallace, and G. C. Hegerl (2000), Annular modes in the extratropical circulation. part II: Trends, *J. Clim.*, *13*, 1018–1036.
Ummenhofer, C. C., A. S. Gupta, M. J. Pook, and M. H. England (2008), Anomalous rainfall over southwest Western Australia forced by Indian Ocean sea surface temperatures, *J. Clim.*, *21*, 5113–5134.
Van den Broeke, M. R., and N. P. M. Van Lipzig (2002), Impact of polar vortex variability on the wintertime low-level climate of East Antarctica: Results of a regional climate model, *Tellus*, *54*, 485–496.
Watterson, I. G. (2000), Southern midlatitude zonal wind vacillation and its interaction with the ocean in GCM simulations, *J. Clim.*, *13*, 562–578.
Yu, L., X. Jin, and R. A. Weller (2007), Annual, seasonal, and interannual variability of air-sea heat fluxes in the Indian Ocean, *J. Clim.*, *20*, 3190–3209.
Yuan, X., and D. G. Martinson (2001), The Antarctic dipole and its predictability, *Geophys. Res. Lett.*, *28*, 3609–3612.
Yuan, X., and C. Li (2008), Climate modes in southern high latitudes and their impacts on Antarctic sea ice, *J. Geophys. Res.*, *113*, C06S91, doi:10.1029/2006JC004067.
Zhou, T., and R. Yu (2004), Sea-surface temperature induced variability of the Southern Annular Mode in an atmospheric general circulation model, *Geophys. Res. Lett.*, *31*, L24206, doi:10.1029/2004GL021473.
Zhu, Y. L., and D. D. Houghton (1996), The impact of Indian Ocean SST on the large-scale Asian summer monsoon and the hydrological cycle, *Int. J. Climatol.*, *16*, 617–632.

J. Li, National Key Laboratory of Numerical Modeling for Atmospheric Sciences and Geophysical Fluid Dynamics, Institute of Atmospheric Physics, Chinese Academy of Sciences, P.O. Box 9804, Beijing 100029, China. (ljp@lasg.iap.ac.cn)
S. Nan and P. Zhao, Chinese Academy of Meteorological Sciences, No. 46, Zhongguancun Nandajie, Haidian District, Beijing 100081, China.
X. Yuan, Lamont-Doherty Earth Observatory, Columbia University, 61 Route 9W, Palisades, NY 10964, USA.